FISEVIER

Contents lists available at ScienceDirect

Developments in the Built Environment

journal homepage: www.sciencedirect.com/journal/developments-in-the-built-environment





Study of properties and behavior of concrete containing EAF slag as coarse aggregate

Nicolás Rojas^a, Marión Bustamante^b, Pedro Muñoz^{c,d}, Karina Godoy^e, Viviana Letelier^{a,*}

- ^a Department of Civil Engineering, Universidad de La Frontera, Temuco, 4780000, Chile
- ^b Doctoral Program in Engineering at the MacroFacultad de Ingeniería UFRO-UBB-UTAL, Chile
- ^c Facultad de Ingeniería, Universidad Autónoma de Chile, Talca, 3460000, Chile
- ^d Universidad Internacional de La Rioja, INeS Research Group, Logroño, 26006, Spain
- e Scientific and Technological Bioresource Nucleus (BIOREN), Universidad de La Frontera, Temuco, 4780000, Chile

ARTICLE INFO

Keywords: Artificial aggregate Concrete Waste recycling Electric arc furnace slag Mechanical properties Physical properties

ABSTRACT

Electric arc furnace slag (EAFS) is an attractive by-product due to its suitability as a replacement aggregate, the use of which helps to reduce the demand for natural resources. The aim of the present study is to determine the suitability of EAFS as a 50% and 100% replacement for coarse concrete aggregates, by evaluating its physical, mechanical and chemical properties. Slump and workability of concretes with EAFS decreased due to the shape and texture of the aggregate. Compressive strength, flexural strength and modulus of elasticity of concretes with EAFS improved by up to 30.9%, 35.7% and 25.0% over the control series, respectively. Absorption, porosity and ultrasonic pulse velocity were favored as well, and the greater density can be beneficial in some cases; however, thermal conductivity and capillary absorption were slightly affected. Considering the good results, EAFS is considered a viable alternative for use as a coarse aggregate replacement in concretes.

1. Introduction

The construction industry is known to be one of the main consumers of natural resources, and concrete is one of the most used construction materials worldwide (Oikonomou, 2005; Xu et al., 2019). Almost 75% of concrete volume corresponds to aggregates, and it is estimated that the global demand for natural aggregates (NA) for construction will see an annual increase of 2.3%, reaching 45,500 million metric tons in 2023 (Anike et al., 2022). This has led to the overexploitation of natural resources in several countries, generating a worrying situation for concrete and its relation to the environment and health. The need for rational management of the reserves, recovery and use of the waste generated by production processes and consumption, have become increasingly important (Ratajczak et al., 2015). It is worth mentioning that sand and gravel production for construction in the United States was about 1 billion tons in 2021, with an increase of 6% over 2020, while industrial sand and gravel production was estimated as 240 billion tons worldwide in the same year (U.S. Geological Survey, 2022). On the other hand, the global steel lag production in 2021 was approximately 190-280 million tons (U.S. Geological Survey, 2022). In addition, the production of 1 ton of steel generates between 130 and 200 kg of slag,

depending on the production process and the composition of the steel, which is then discarded occupying large areas of land and polluting the environment (Rashad, 2019).

Several studies have demonstrated that the characteristics and properties that NA contribute can also be obtained from certain byproducts, which can be used as NA replacements, as coarse and fine aggregates in concrete production (Abendeh et al., 2022; Ashish and Verma, 2021) or, even, as a binder in cement (Revilla-Cuesta et al., 2022; Ashish and Verma, 2019). In this way, it is expected that a part of the environmental, economic and social impact that accompanies the exploitation of NA will be mitigated (Santamaría et al., 2021). In this sense, the use of electric arc furnace slag (EAFS) as a partial or total substitute for fine and coarse NA in concrete manufacturing is an alternative with promising results for the construction industry, specifically for concrete mixers (De Domenico et al., 2018).

EAFS is a by-product of the iron and steel industry obtained from an electric arc furnace as a result of the addition of flux at 1700 °C, with steel scrap being the main raw material. Its basic characteristics include a relatively high mass resulting from its internal composition, ranging between 3000 and 4000 kg per cubic meter (Santamaría et al., 2022). EAFS mainly contains iron oxides, silicates, and calcium aluminates. Its

E-mail address: viviana.letelier@ufrontera.cl (V. Letelier).

^{*} Corresponding author.

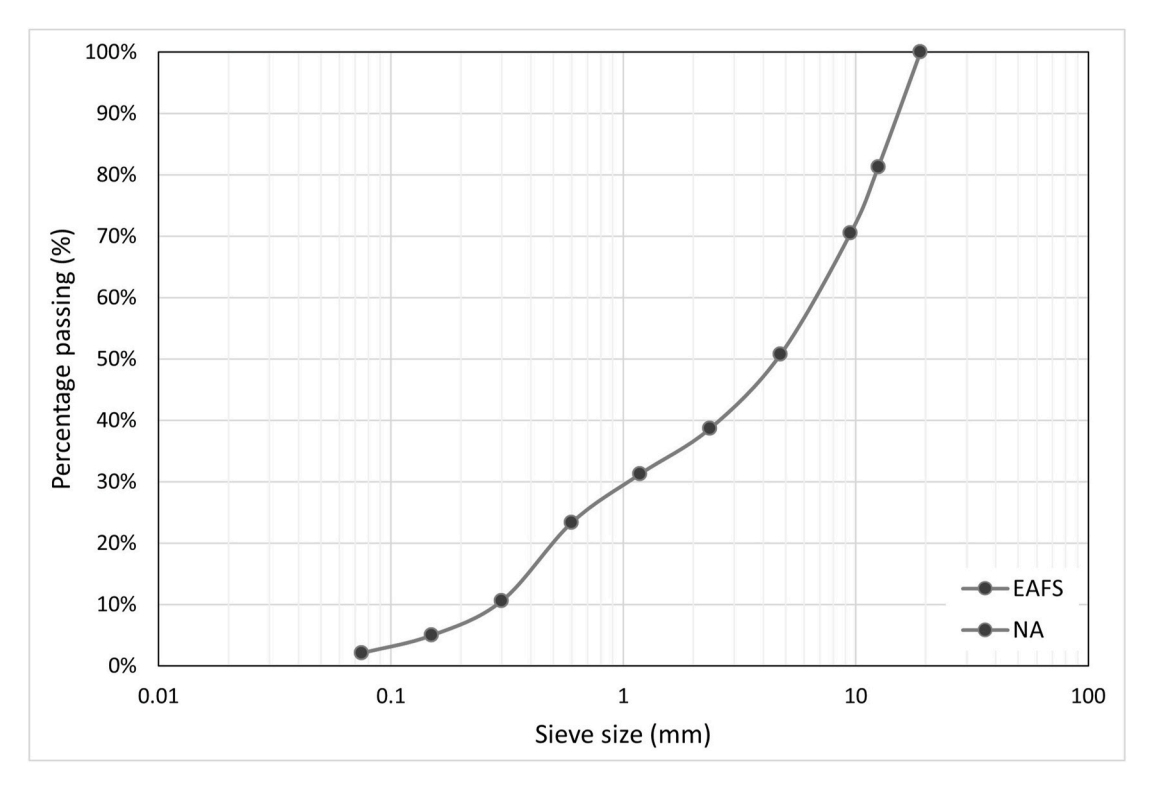


Fig. 1. Particle size distribution used for NA and EAFS.

main properties are its hardness, tenacity, resistance to abrasion, chemical stability, good durability and high density (Santamaría et al., 2021). As such, several researchers consider that it can be used in concrete manufacturing without any problems by replacing heavy and fine NA according to the required particle size (Santamaría et al., 2022; Zanini, 2019; Arribas et al., 2015).

Consequently, various studies have been conducted to determine the different properties of EAFS and to evaluate its behavior in concretes. Brand and Roesler (2015) studied the compressive strength of concretes with basic oxygen furnace (BOF) slag and EAFS. The authors reported that the aggregates from EAFS were more angular and rougher than aggregates from BOF slag, generating an interfacial transition zone (ITZ) of better quality and, thereby, contributing to a better mechanical performance in the form of strength, rigidity and tenacity (Pellegrino and Gaddo, 2009; Martins et al., 2021). In addition, several authors have obtained favorable results regarding the mechanical properties of concrete with EAFS, such as greater compressive strength, flexural strength and modulus of elasticity (Qasrawi et al., 2009; Faleschini et al., 2015; Jagadisha et al., 2021).

Another important point to consider is the permeability of the concrete, which largely affects the durability of the material (Zhang et al., 2019; Wang et al., 2013). Saxena and Tembhurkar (2018) demonstrated that the use of EAFS as a NA replacement notably improves the durability and density in the microstructure. Other studies indicate that under aggressive environmental conditions like freeze/thaw cycles or exposure to chlorides, the durability of the concrete can be improved by substituting NA for EAFS (Faleschini et al., 2015; Pellegrino et al., 2013; Manso et al., 2006). However, in extreme environmental zones these performances depend on the physical and chemical characteristics of the slag, because these are affected by the composition of the scrap in the iron and steel plant, as well as in the steel manufacturing and cooling processes. It is worth noting that the cooling speed and the foamy slag formation phase not only influence porosity, but also its classification, expansion potential and mineralogical composition (De Domenico et al., 2018). In this regard, Geiseler (1996) and Motz and Geiseler (2001) used EAFS to manufacture concrete. They mention certain limitations associated with high replacement percentages, linked to the swelling of the free calcium oxide (CaO) and magnesium oxide (MgO) present in the aggregate. Similarly, Santamaría et al. (2018) reported that CaO and MgO are mainly responsible for both the hydration and expansion phenomena inherent to these slags, once they are in contact with water, the CaO is quickly hydrated, causing a gradual expansion over a longer time period. Nevertheless, Manso et al. (2006) and Pellegrino and Gaddo (2009) showed that this phenomenon can be easily prepared using a suitable stabilization treatment applied to the furnace slag, exposing it outdoors for three months and with daily moistening/drying cycles for one week.

Considering these factors, the use of EAFS as an aggregate in the concrete is a favorable alternative, because it can improve the mechanical properties of conventional concretes. In spite of this, Coppola et al. (2016) described one of the disadvantages of EAFS being its high density, causing fresh concrete to be less workable, making its use difficult in cantilever elements but suitable for foundations. In this sense, an alternative to mitigate its low workability is to use superplasticizers (SP).

In the present study, the EAFS from a national company was characterized and compared with natural aggregates. Then, tests were conducted to determine the mechanical, physical and chemical properties of the EAFS in concretes as a coarse aggregate replacement in proportions of 50% and 100%. The EAFS aggregate was compared with conventional concrete, in order to evaluate its behavior and potential. Based on these results, the idea was to assess the integration of a by-product of the iron and steel industry in sustainable concrete manufacturing and reduce the environmental impact of natural aggregate extraction. By considering the slow progress at a national level compared to other more developed countries (in term of recycled aggregates, concrete investigation, and the management and reuse of construction and demolition waste (CDW) in the industry), the results obtained in this investigation are of great interest to make construction more environmentally friendly while aiming for a circular economy. In addition, taking into account the fact that some companies are investing in new construction practices in order to reduce waste generation (trying to reuse some of them), this and

Table 1 Physical properties of the aggregates.

Aggregate type	Specific gravity (OD)	Specific gravity (SSD)	Apparent specific gravity	Water absorption (%)	LA abrasion loss (%)
CNA	2.69	2.65	2.75	1.40	19.93
FNA	2.54	2.48	2.62	2.17	_
EAFS	3.27	3.21	3.42	1.96	20.60

further studies highly enrich the academic knowledge in the country, making contributions to the valorization of CDW that can benefit both the industry and the environment.

2. Materials and characteristics

2.1. Cement

Portland-Pozzolanic cement was used according to ASTM C595M - 21 (ASTM C595/C595M - 16, 2021). This cement was formulated with clinker, pozzolan and plaster, dosed precisely and controlled in a joint grinding process of stable quality and minimal variability. According to its technical datasheet, the initial setting time was 180 min and the final setting time was 240 min. It also presents a specific Blaine surface equal to 4100 $\rm cm^2/g$ and a specific weight of 2.81 g/cm³. In terms of its compressive and flexural strength, these were 230 kg/cm² and 45

 kg/cm^2 at 7 days, and 340 kg/cm^2 and 62 kg/cm^2 at 28 days, respectively.

2.2. Aggregates

In this study, natural siliceous gravel and sand from southern Chile were used. The NA had particle sizes from 2.36 mm to below 0.075 mm for sands, and from 19 mm to 4.75 mm for gravels. In terms of the replacement aggregate, only the coarse part of EAFS was used, to the same sieve sizes as the NA. The EAFS came from a national company that uses recycled steel in its production processes; it was subjected to an aging process and exposed to the elements for three months. The granulometric distribution of the aggregates presented in Fig. 1 was carried out in accordance with ASTM C136/C136M - 19 (ASTM C136/C136M - 19, 2019). Also, Table 1 details the physical properties obtained from the methodology available in ASTM C127-15 (ASTM C127-15, 2015) and ASTM C128-15 (ASTM C128-15, 2015) for the specific gravity and water absorption in gravel and sands, respectively. In addition, to determine the resistance to abrasion and impact for both of the aggregates using the Los Angeles machine method, ASTM C131/C131M - 20 was considered (ASTM C131/C131M - 20, 2020). The results obtained for the EAFS aggregate were comparable with NA (20.60% and 19.93%, respectively), which indicates a good quality and durability of the aggregate, avoiding undesirable strength losses due to possible fracturing. The angularity number of the NA and EAFS was also determined,

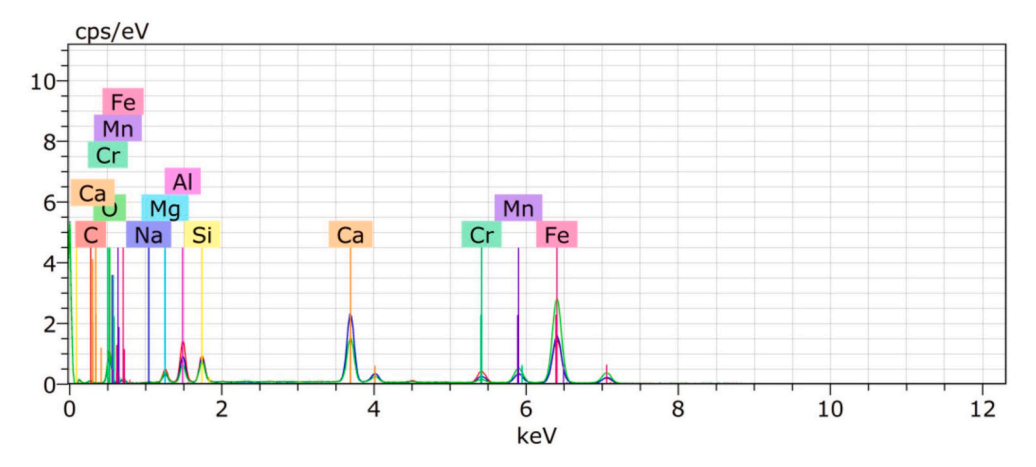


Fig. 2. EDS of EAFS aggregate.





Fig. 3. Aggregates used for the fabrication of the concrete specimens. (a) EAFS and (b) NA.

Table 2 Spectrum of EAFS aggregate EDS.

Spectrum	С	0	Na	Mg	Al	Si	Ca	Cr	Mn	Fe
Mean value	4.43	27.67	0.59	3.62	7.40	4.15	13.79	2.59	4.67	31.26

Table 3Mixture proportions of concrete (kg/m³).

Sample	Water	Cement	w/c ratio	Coarse NA	Coarse EAFS	Fine NA	SP
C00	183.51	382.31	0.48	1061.40	0	772.23	7.65
EAFS-50	183.51	382.31	0.48	530.70	659.63	772.23	7.65
EAFS-100	183.51	382.31	0.48	0	1319.25	772.23	7.65

as per the procedure mentioned in IS 2386 (IS 2386, 1963), and was found to be 2 and 5, respectively, which was supported by the information reported by (Singh et al., 2022). This means that EAFS was less rounded than NA, thus affecting its concrete workability. Three types of concrete series were analyzed, which replaced coarse NA (CNA) for EAFS at 0%, 50% and 100%. The particle size of the NA stayed the same for all of the series.

With respect to the artificial aggregate, Fig. 2 shows its EDS assay, while Table 2 shows its spectrum. This analytical technique allows the chemical characterization of the EAFS and the sample mainly consists of iron which indicates its high resistance to corrosion and hardness. The sample also consists of oxides, mainly oxygen with Ca, C, Mg and Al, among others. This analysis shows the presence of Cr and Mn, which are related to the raw materials in the steel production process, from which the EAFS was obtained. Fig. 16 also shows the X-ray diffraction (XRD) of the slag aggregate, which is in agreement with the EDS test showing peaks associated with gehlenite (Ca2Al(SiAl)O7), wüstite (FeO), å kermanite (Ca₂MgSi₂O₇), calcite (CaCO₃) and spinel (MgAl₂O₄). The thermogravimetric analysis (TGA) of the slag used (see Fig. 18) was also performed, where two peaks were observed between 650 and 850 °C, which is associated with the decomposition of the calcite. This is due to the fact that the slag spent three months in the environment and, therefore, in contact with water and CO₂, giving way to the formation of CaCo3 from Ca(OH)2.

2.3. Superplasticizer (SP)

In the preparation of all the series (C00, EAFS-50, EAFS-100), a superplasticizer (SP) was used to achieve greater plasticity in the fresh state. This additive also generated a reduction in the mixing water content and, therefore an increase in strength in the early stages, improving permeability and durability parameters in the concrete. This additive has a density of $1.20\pm0.02\,kg/l$. For application effects, the SP was diluted in the mixing water immediately before the concrete fabrication, in a proportion of 2% in weight of the dosed cement. In addition, fine aggregate was increased by 10% for each particle size to compensate for the water reduction and maintain the homogeneity of the fluid mixture according to the recommendations in the technical datasheet of the product.

3. Experimental program

3.1. Mixture proportions

For the purposes of this study, concretes were manufactured with a compressive strength of 30 MPa, considering different percentages of EAFS replacing coarse natural aggregate. A control series (C00) was prepared, only with NA, and two series with replacement of EAFS by the CNA in percentages of 50% and 100%, called EAFS-50 and EAFS-100, respectively. With regard to the fine aggregate, only NA was used for all series. Table 3 presents the dosage for each of the series, maintaining

the same w/c ratio for all of them. For each series, six 15 cm \times 30 cm cylindrical specimens, three 10 cm \times 15 cm cylindrical specimens and three 15 cm \times 15 cm \times 55 cm prismatic specimens were made.

Considering the higher specific gravity of EAFS over NA, the substitution of the aggregate was made by volume using a relation between the apparent specific gravity of both materials. In this way, when dosing the material, the volumes of NA and EAFS as the replacement aggregate were equal, regardless of their difference in apparent specific gravity.

3.2. Test methods

3.2.1. Compressive strength

The test was carried out using the rupture by compression of cylindrical specimens, as proposed by ASTM C39/C39M - 21 (ASTM C39/C39M - 21, 2021). The conditioning and curing of each specimen was undertaken according to ASTM C31/C31M - 19 (ASTM C31/C31M - 19, 2019). The test was applied with a continuous loading speed of 0.25 \pm 0.05 MPa/s until the specimen ruptured. Three identical samples of 15 cm \times 30 cm were tested for each series, in order to generate representative results. Each series was tested after 7 and 28 days of curing.

3.2.2. Modulus of elasticity

The modulus of elasticity was tested according to ASTM C469M - 14 (ASTM C469/C469M - 14, 2014) using the compression test of three cylindrical specimens of 15 cm \times 30 cm with 28 days of curing; a compressometer/extensometer was coupled to enable pertinent calculations.

3.2.3. Flexural strength

The flexural strength test to rupture of the prismatic concrete specimens was carried out according to ASTM C78-18 (ASTM C78/C78M - 18, 2018). For each series, three identical 15 cm \times 15 cm \times 55 cm samples were tested with 28 days of curing.

3.2.4. Density, absorption and porosity

The density, absorption and porosity of the concrete were obtained for each series according to ASTM C642-21 (ASTM C642-21, 2021). For this test, the submerged, wet or saturated and dry masses of the specimens were determined, and the parameters indicated in the standard were obtained. Nine cylindrical specimens, 100 mm in diameter and 50 mm in height, with 28 days of curing were used.

3.2.5. Capillary absorption

The initial capillary water absorption rate was determined according to ASTM C1585-20 (ASTM C1585-20, 2020). The method consists of recording the gain in mass of a sample comprised of a slice of concrete subjected to the action of one of its sides coming into contact with water. The water absorption rate (mm/s $^{1/2}$) was determined from the slope traced for the data collected between 1 min and 6 h. For each test, nine cylindrical samples, 100 mm in diameter and 50 mm in height, with 28

Table 4 Slump of concrete mixes.

Sample	Slump (mm)			
C00 EAFS-50	80 60			
EAFS-100	30			

days of curing were tested.

3.2.6. Thermal conductivity

To determine the thermal conductivity of the concrete, non-destructive testing was carried out for each series using the thermal probe procedure with a Hot Disk TPS 1500 thermal conductivity equipment as per ISO 22007-2 (ISO 22007-2:2008(E), 2008). Three cylindrical specimens, 100 mm in diameter and 50 mm in height, with 28 days of curing were tested for each series. After drying, the samples were kept at a temperature of 20 $^{\circ}\text{C}$ for testing.

3.2.7. Ultrasonic pulse velocity (UPV)

The ultrasonic pulse velocity (UPV) method was used according to ASTM C597-16 (ASTM C597-16, 2016), to verify the homogeneity of the concrete, the presence of voids or fissures, possible changes over time, and to determine the physical characteristics and dynamics of the material (Letelier et al., 2021). This test consists of determining the time that a wave takes to cross through a sample, and based on this, the pulse velocity is calculated. The device used for this test was the PULSONIC 58-E4900 (Controls Group). For each series, nine cylindrical specimens, 100 mm in diameter and 50 mm in height, with 28 days of curing were tested.

3.2.8. X-ray diffraction (XRD)

For the XRD analysis, a 15 cm \times 30 cm cylindrical specimen was cured for 28 days. Then, to obtain the samples needed, a 2 cm slice was cut from it and crushed with a hammer to obtain different pieces, which were then dried in an oven at 60 $^{\circ}$ C. These were subsequently crushed again using a mortar, until a powder smaller than 0.075 mm was

obtained. After the samples were conditioned, the test was performed using the Bruker D2 PHASER equipment with an X-ray tube (Cu 1.54 Å). The diffractogram was obtained in a range of 2θ , varying from 10° to 80° and at a rate of 1 s for 60 min.

3.2.9. Scanning electron microscope (SEM)

To examine the microstructure of the samples of each series, a scanning electron microscope (SEM) was used, equipped with a back-scattered electron detector (BSE) and an energy-dispersive spectrometer (EDS). In this case, the samples were processed with HITACHI SU3500 equipment, applying a voltage of 10 kV and a working distance of 12 ± 0.2 mm. As for the XRD test, the samples came from a 15 cm \times 30 cm cylindrical specimen cured for 28 days. An approximately 1 cm wide slice was extracted from the specimen and crushed with a hammer to obtain smaller pieces. For each series, a sample was analyzed in three zones, taking magnifications at 500, 200, 100, 50, 20 and 10 μm .

3.2.10. Thermogravimetric analysis (TGA)

In the thermogravimetric analysis, the mass of the sample was tested at different temperatures using a Q600 simultaneous thermal analyzer with a heating speed of 20–1000 $^{\circ}\text{C}$ for 10 min. The derivative of the TG curve was determined to obtain the DTG curve, which provides results on the mass loss with the increase in temperature. The sample tested came from the same 15 cm \times 30 cm cylindrical specimen used for the XRD and TGA tests. A 2 cm high slice was extracted, reducing the sample with the help of a mortar until a powder smaller than 0.075 mm was obtained.

4. Results and discussion

4.1. Fresh concrete properties

The workability of the fresh concrete was determined using the slump test, according to ASTM C143/C143M - 20 (ASTM C143/C143M - 20, 2020). The values expressed in Table 4 reflect the workability of the mix in a fresh state associated with a slump in each series for the preparation of the specimens.

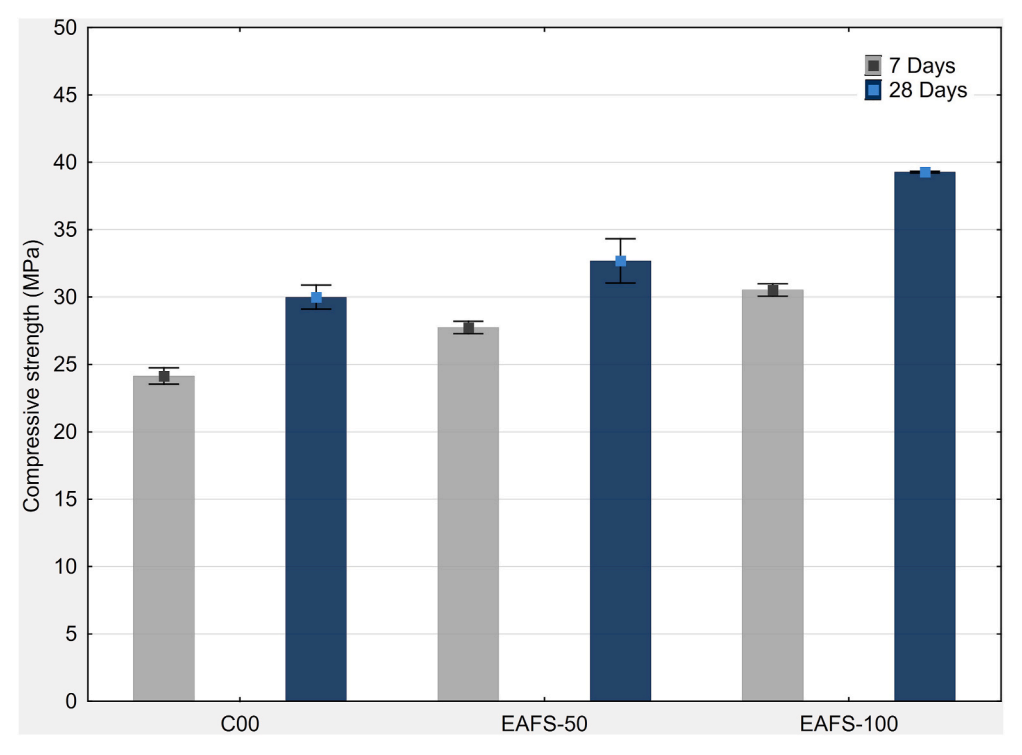


Fig. 4. Compressive strength of concrete specimens at 7 and 28 days.

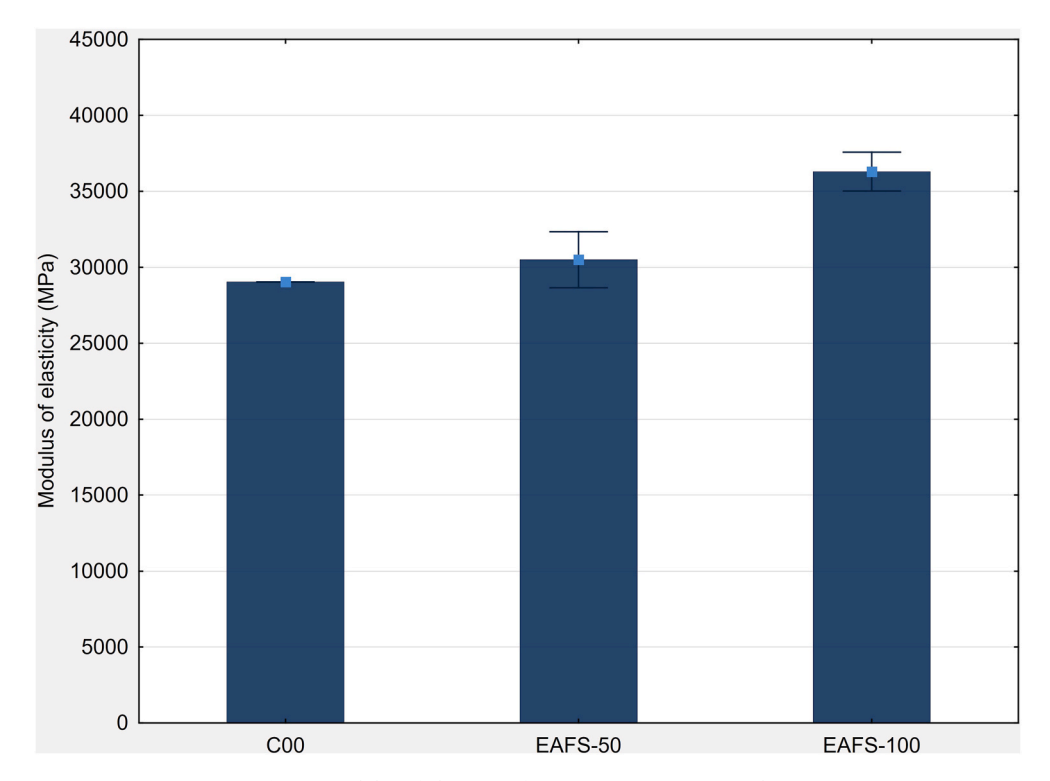


Fig. 5. Modulus of elasticity of concrete specimens at 28 days.

Generally speaking, a gradual reduction in the workability can be observed as the percentages of coarse replacement aggregate are increased. This difference is mainly due to the EAFS being more angular, with a rough surface texture compared to the NA, which had a smoother and rounder surface. However, even though the slump was significantly reduced for the series with full EAFS replacement, no significant loss of workability on the fresh mixtures was noted due to the SP. Fig. 3

indicates that the porosity of the EAFS is considerably greater than that of the NA. This difference is attributed to its production process, specifically its cooling, since, after it is taken out of the high-temperature furnace, it is placed in an area outside which is open to the weather, generating angular, porous particles with a rough surface (Papachristoforou et al., 2020).

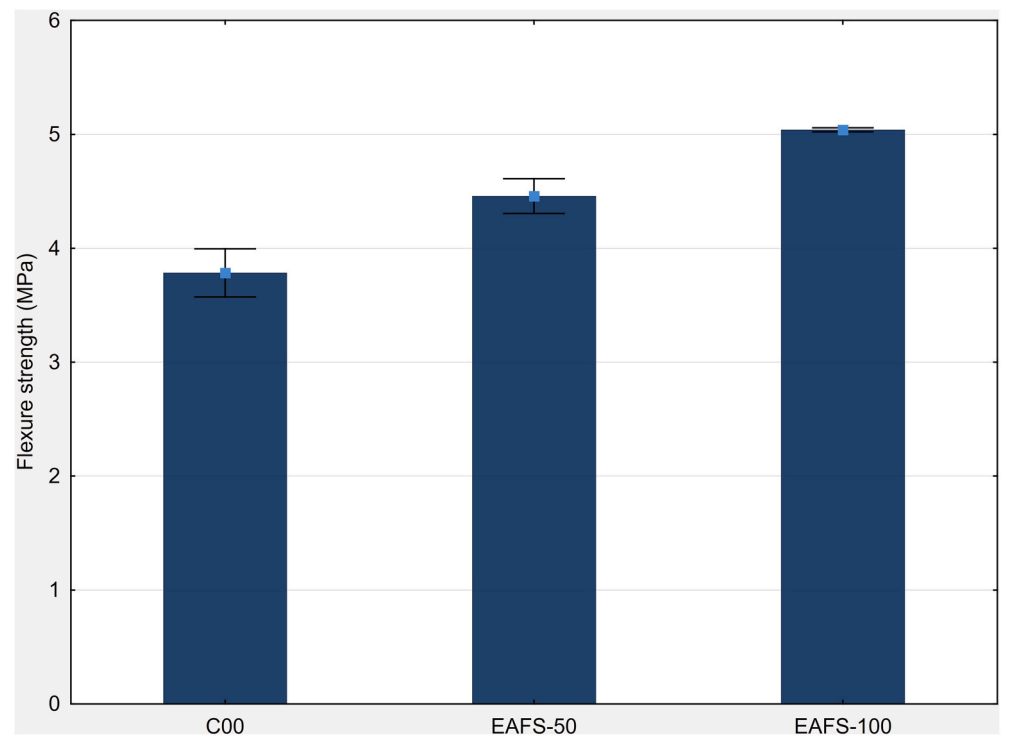


Fig. 6. Flexural strength of concrete specimens at 28 days.

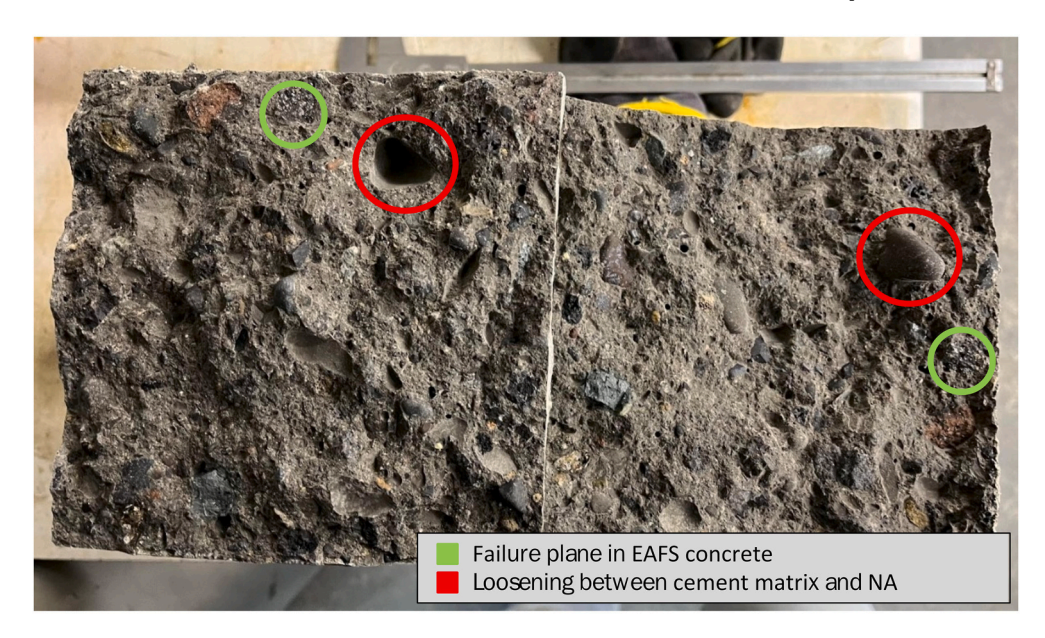


Fig. 7. Flexural failure plane of prismatic specimen.

4.2. Compressive strength

Fig. 4 shows the development of the average compressive strength obtained from three specimens per series, with 7 and 28 days of curing. The compressive strength surpassed the design strength, since for both the EAFS-50 and EAFS-100 series, the compressive strength was over 30 MPa. At 7 days, there was an increase of 14.95% and 26.47% in the compressive strength when it was replaced with 50% and 100% of EAFS, respectively. On the other hand, at 28 days the strength increased by 8.97% and 30.90% for the series with 50% and 100% replacement compared to the control series.

The increase in compressive strength of the series with EAFS compared to the control series is attributed to the textured surface and

better mechanical properties of the EAFS aggregate. This means that the rougher surface and higher angularity of EAFS over NA contributes to an increasing bond between the cement paste and the aggregate particles, improving the concrete quality and, consequently, resulting in a higher compressive strength (Qasrawi et al., 2009; Coppola et al., 2016). Furthermore, the improved strength is linked to a higher pozzolanic reactivity and the development of a denser ITZ (Jagadisha et al., 2021). For Rashad (2022) and Monosi et al. (2016), the porous nature of the slag aggregate that enables it to absorb the internal water of the mixture reduces the evaporated water indices, contributing to an internal curing that aids in the continuous hydration process of the binder, which could condition it for the development of greater strengths.

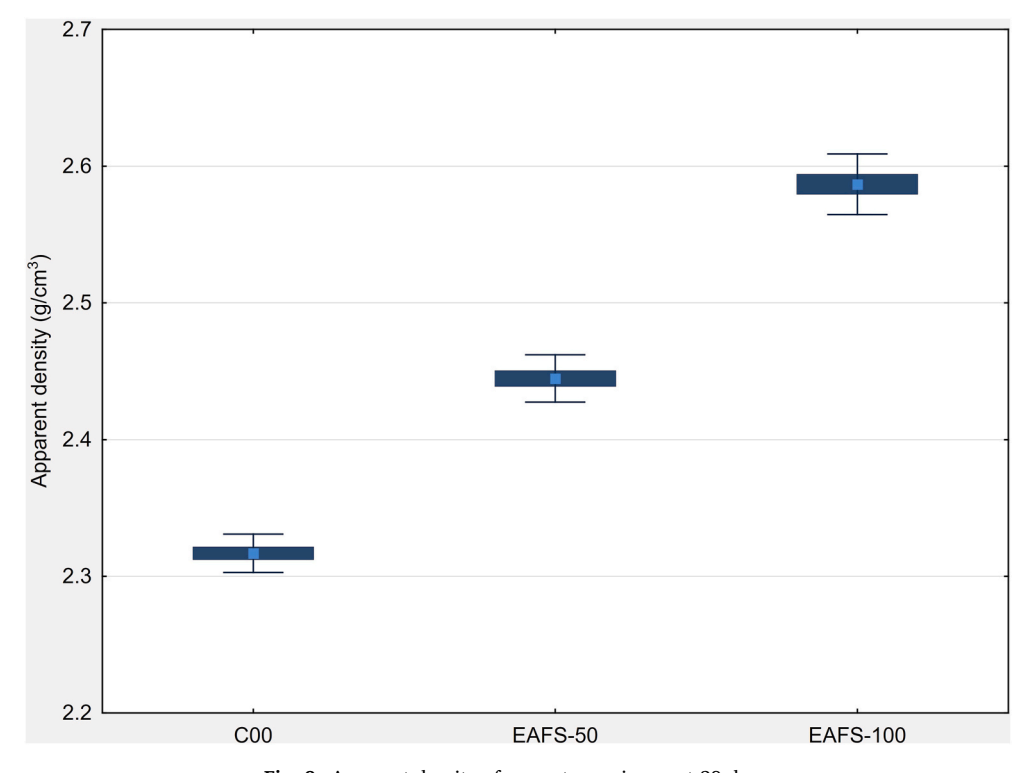


Fig. 8. Apparent density of concrete specimens at 28 days.

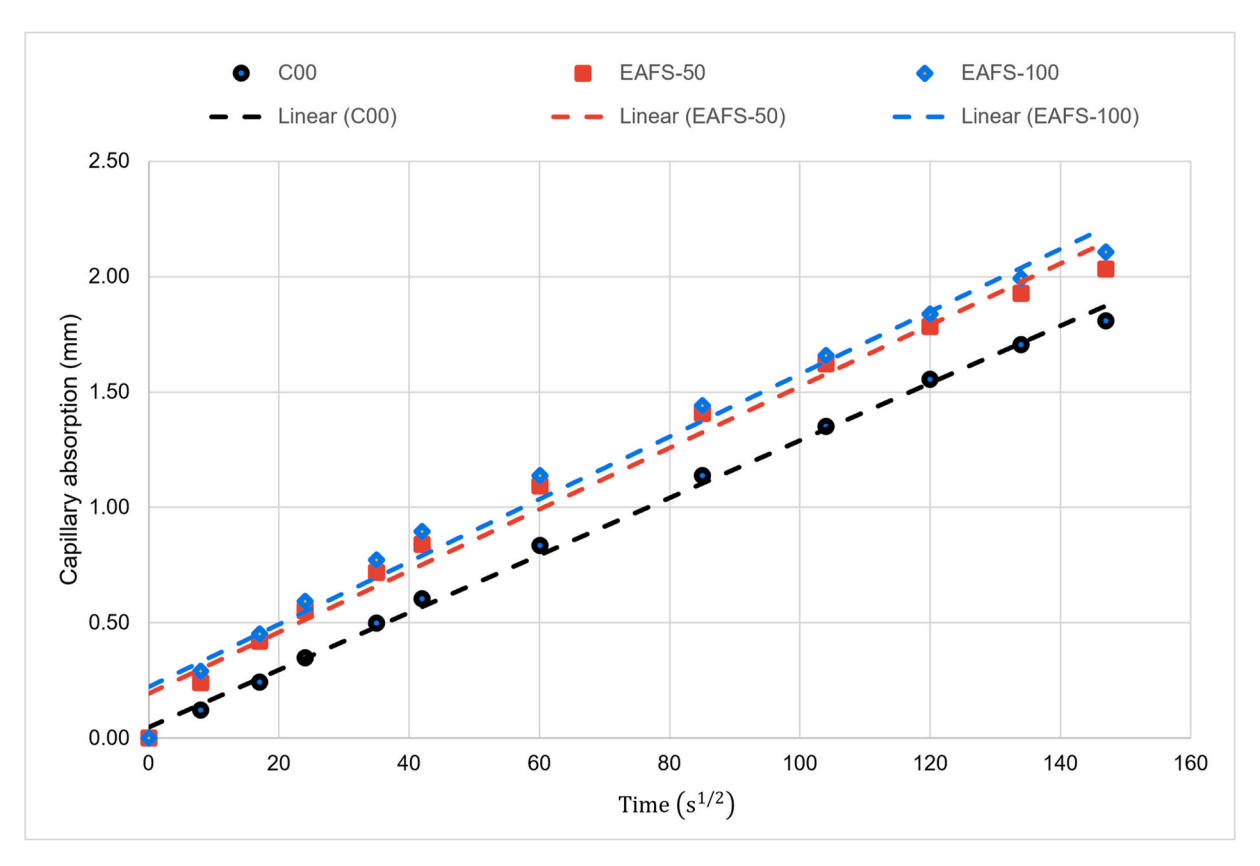


Fig. 9. Initial capillary absorption curves of concrete specimens at 28 days.

4.3. Modulus of elasticity

Fig. 5 provides the average results corresponding to the modulus of elasticity for the C00, EAFS-50 and EAFS-100 series, whose values were 29,035 MPa, 30,500 MPa and 36,300 MPa, respectively. This means that replacing NA with EAFS at 50% and 100% achieved an increase of 5.05% and 25.02% with respect to the control series. Pellegrino and Gaddo (2009) indicated that a greater cohesion between the aggregate and the cement matrix may produce greater rigidity in the concrete resulting from the great roughness of EAFS.

4.4. Flexural strength

Fig. 6 shows the development of the average flexural strength obtained from three specimens per series with 28 days of curing. Similar to that obtained in the compression test and the modulus of elasticity test, the flexural strength also has an ascending behavior as the presence of EAFS increases in the concrete. The concrete with EAFS had an increase of 17.99% and 35.71% at 28 days for the series with 50% and 100% replacement compared to the traditional concrete (which reached a strength of 3.78 MPa).

This behavior is attributed to a better adhesion between the aggregates and the cement matrix as a result of the physical properties present in EAFS (Faleschini et al., 2015; Pellegrino et al., 2013; Adegoloye et al., 2015). In Fig. 7, it is observed that for the series with 50% in most cases the division occurred within EAFS, unlike the NA, where this occurred between the cement matrix and the aggregate. This is why the influence of the ITZ observed in Fig. 15 could have contributed to a greater flexural strength than the reference series. In general, EAFS mixes tend to have a better flexural strength due to the texture and superior bonding of the artificial aggregate with the ITZ because of its interaction and better mechanical characterization of the EAFS aggregate compared to NA (Saxena and Tembhurkar, 2018). Brand and Roesler (2018) found that,

unlike basic oxygen furnace (BOF) slag which, exhibits two different layers, EAFS had a single layer; this implies a better mechanical bond with the cement paste, leading to a better microstructure and higher strengths than dolomite aggregates. Additionally, Papachristoforou et al. (2020) reported that the irregular surface of the EAFS particles and a high density contribute to better adhesion to the cement matrix compared to the NA, providing the concrete with better flexural properties.

4.5. Density

As illustrated in Fig. 8, the densities at 28 days of hardened concretes with 50% and 100% of EAFS significantly increased compared to the control series, which is directly related to the high density of the EAFS as granular material. While the control series had a density of 2.32 g/cm³, the EAFS-50 and EAFS-100 had densities of 2.44 g/cm³ and 2.59 g/cm³, respectively. On the other hand, the theoretical density of the concrete mixes for the C00, EAFS-50 and EAFS-100 were 2.40 g/cm³, 2.53 g/cm³ and 2.66 g/cm³, respectively. It should be noted that the theoretical densities are greater than those for specimens tested at 28 days, which is similar to other studies (Jagadisha et al., 2021; Santamaría et al., 2020; Lim et al., 2019). This could be because of the aggregate shape, in addition to voids and air trapped in the concrete mixes, leading to a small decrease in concrete density.

This behavior is attributed directly to the relation between the EAFS as a replacement material and its density. As noted in Table 1, the EAFS presents a specific gravity significantly greater than the NA, reaching a 17% difference. These results are consistent with the literature, specifically Abu-Eishah et al. (2012), and that could be an advantageous property for those applications where the weight is an important factor.

Table 5Initial capillary absorption slope of concrete specimens at 28 days.

Sample	Slope (mm/s ^{1/2})
C00	0.01212
EAFS-50	0.01290
EAFS-100	0.01308

4.6. Capillary absorption

The initial capillary absorption results presented in Fig. 9 show that at 28 days of curing the capillary absorption rate was slightly greater for the series that contain EAFS. From Table 5 it can be seen that the series made with 50% and 100% replacement obtained an increase of 6.44% and 7.92% compared to the control series that obtained an average of 0.0121 $\,\mathrm{mm/s^{0.5}}$.

Biskri et al. (2017) indicate that capillary absorption is mainly related to the capillary voids and EAFS, beacause it is a more porous material by nature, and promotes earlier water absorption in the concrete, unlike the NA, which is a smooth material with a long-term absorption tendency. Although the porosity of the concrete is inferior with the presence of EAFS, according to the same author, the short duration of the testing does not allow for a total filling of the voids in the sample. Ortega-López et al. (2018) mentioned that the size and distribution of the pores also influence the speed of capillary absorption in the concrete. The increase in capillary absorption for concretes with EAFS was less than 2% compared to the control series, which is why it does not generate a significant impact. A similar effect was reported by Özalp (2022), who determined that although there is a slight increase in the capillary absorption with the incorporation of EAFS into the concrete mixtures, the permeability is sufficient to limit the entry of harmful agents, such as chloride ions, that affect the structure.

4.7. Water absorption and porosity

As shown in Fig. 10, water absorption decreased as the presence of

EAFS in the concrete (with 28 days of curing) increased. The control samples absorbed an average of 4.48%, whereas, for the samples of the series with 50% and 100% replacement of EAFS for NA, they absorbed an average of 4.11% and 3.68% respectively. This reduction in the water absorption can be attributed to the capacity of the cement matrix to fill the pores of the EAFS particles, generating a denser surface, which further hinders the penetration of water through concrete surfaces (Singh et al., 2022; Khalaf et al., 2020). In addition, less water absorption leads to greater compressive strength (Jagadisha et al., 2021), which agrees with the results in Fig. 4.

With respect to the porosity of the concrete observed in Fig. 10, this also decreases as the replacement rate of EAFS for NA increases. The concrete with NA obtained an average porosity of 10.39%, whereas the concretes with EAFS were 10.05% and 9.53% for the series with 50% and 100% replacement, respectively. The porosity presents a reduction of 8.28% between the control series and a total EAFS replacement. This is consistent with the SEM images (see Figs. 14 and 15), where a smaller porosity is observed on the surface of the aggregate. Despite the greater porosity of the EAFS aggregate shown in Fig. 3a compared to the NA in Fig. 3b, the subsequent reduction in the porosity of the concrete with EAFS could be due to the better bond with the cement matrix, thus improving its surface properties (Singh et al., 2022).

4.8. Thermal conductivity

The average thermal conductivity is shown by series in Fig. 11. The control series obtained an average thermal conductivity of 1.35~W/mK, whereas values of 1.40~W/mK and 1.44~W/mK were obtained for the EAFS-50 and EAFS-100 series, respectively.

Letelier et al. (2021) and Marie (2017) studied the thermal behavior of mortars and concretes with recycled aggregate, where a close relation between density and thermal conductivity was determined. As the density becomes greater, the thermal conduction of the concrete will be greater as a result of the pore reduction, considering that air is a good thermal insulator (Ahmad et al., 2017). Compared to traditional concrete, the samples with EAFS, with less porosity (see Fig. 10) and greater

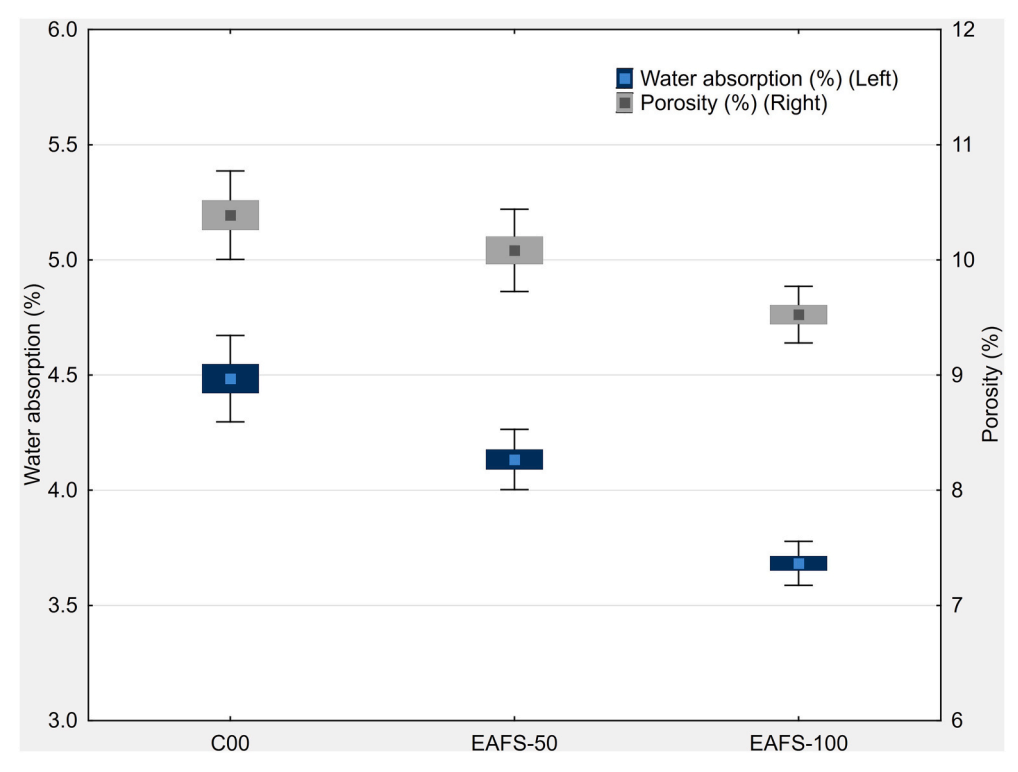


Fig. 10. Water absorption and porosity of concrete specimens at 28 days.

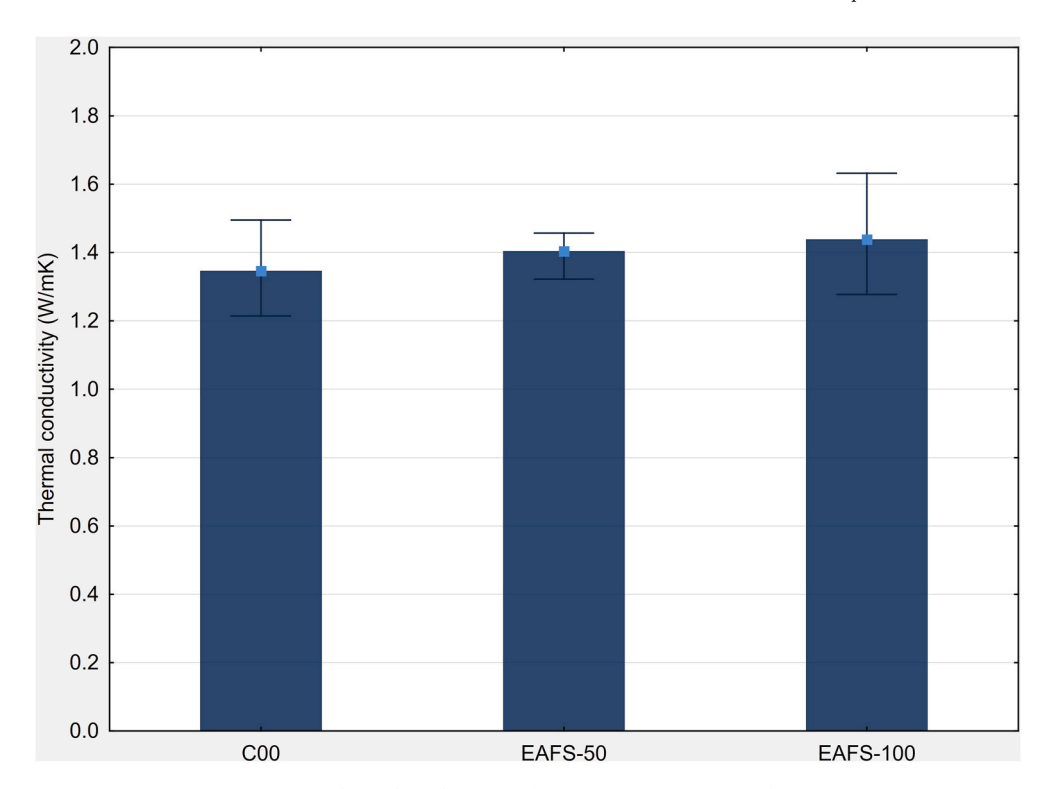


Fig. 11. Thermal conductivity of concrete specimens at 28 days.

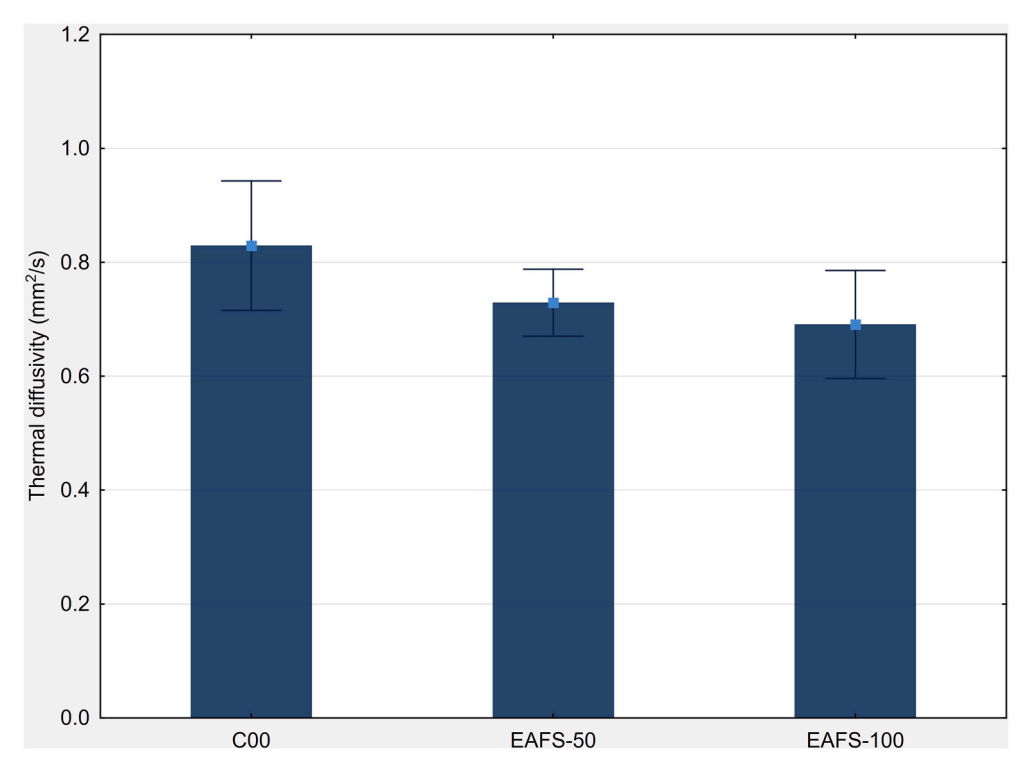


Fig. 12. Thermal diffusivity of concrete specimens at 28 days.

density (see Fig. 8), allow greater thermal conductivity within the matrix, increasing by 4.23% and 6.84% for EAFS-50 and EAFS-100, respectively. In addition, the nature of EAFS providing high percentages of iron (around 20–30%) and aluminum in its chemical composition allow for greater thermal conductivity in the concrete through the EAFS (Andrade et al., 2021).

Although the concrete with EAFS has a greater capacity for thermal

conduction, Fig. 12 shows that for the series with 50% and 100% replacement, the thermal diffusivity coefficient falls by 12.06% and 16.65%, respectively, compared to the control series. EAFS generates slower heat propagation in the concrete than in the NA. This means that, under certain extreme climatic conditions, the concrete with EAFS will take longer to warm up or cool down, but it will undergo greater temperature changes than traditional concrete in the long term.

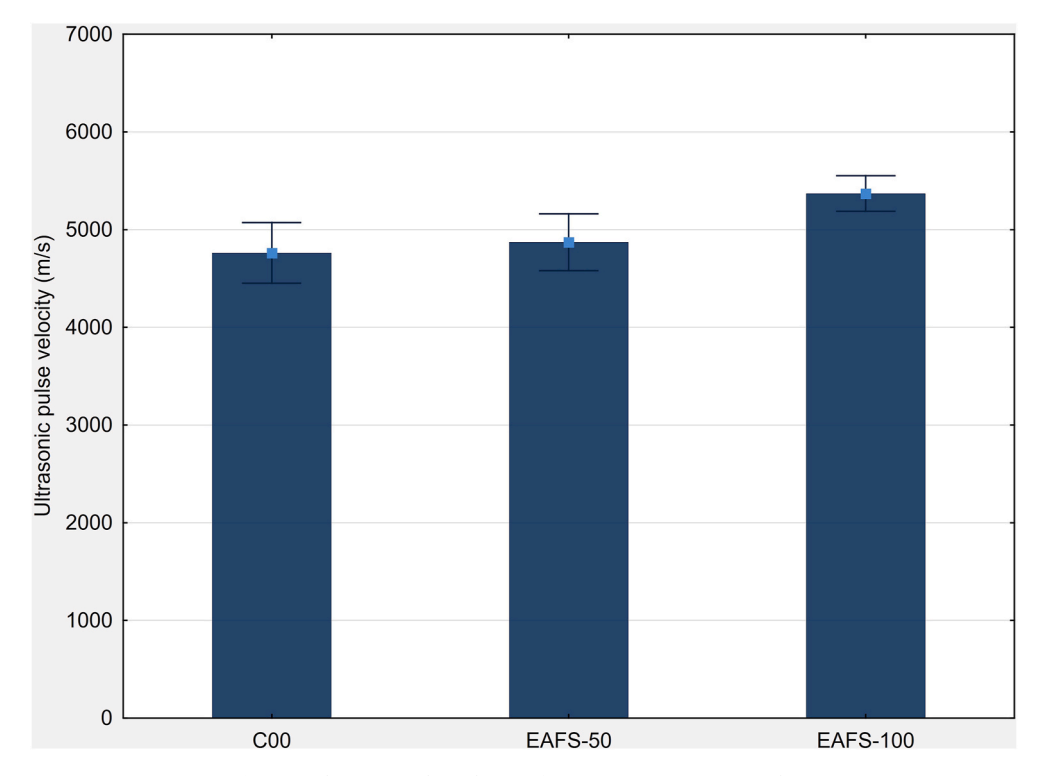


Fig. 13. Ultrasonic pulse velocity of concrete specimens at 28 days.

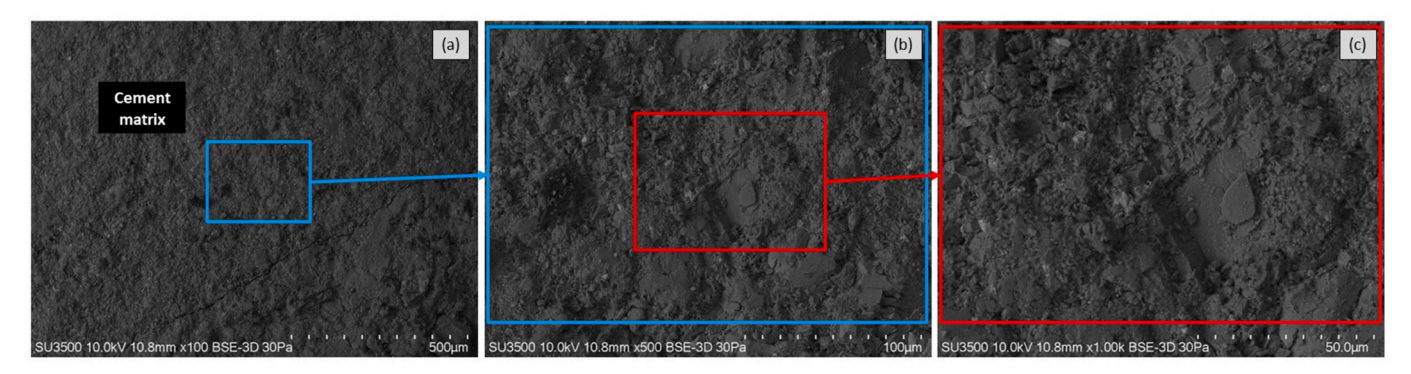


Fig. 14. SEM image of EAFS-50 concrete.

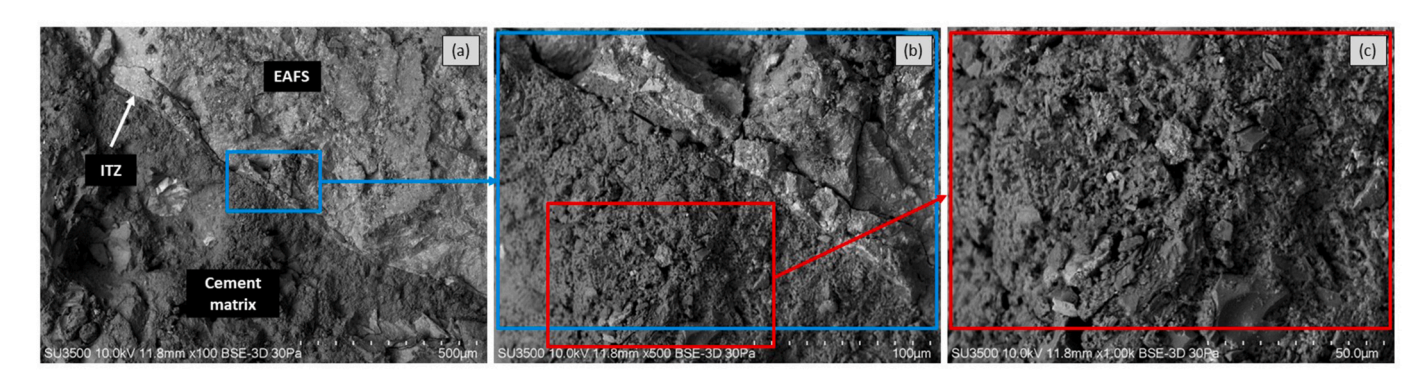


Fig. 15. SEM image of EAFS-100 concrete.

4.9. Ultrasonic pulse velocity (UPV)

According to Fig. 13, the average pulse velocity by series increased as the percentage of NA replacement increased. The pulse velocity for the

control series was 4695 m/s, whereas, in concretes with EAFS it was 4928 m/s and 5370 m/s with 50% and 100% replacement, respectively. For both the control series and the series with EAFS, being above 4500 m/s is considered excellent, according to the classification of the IS

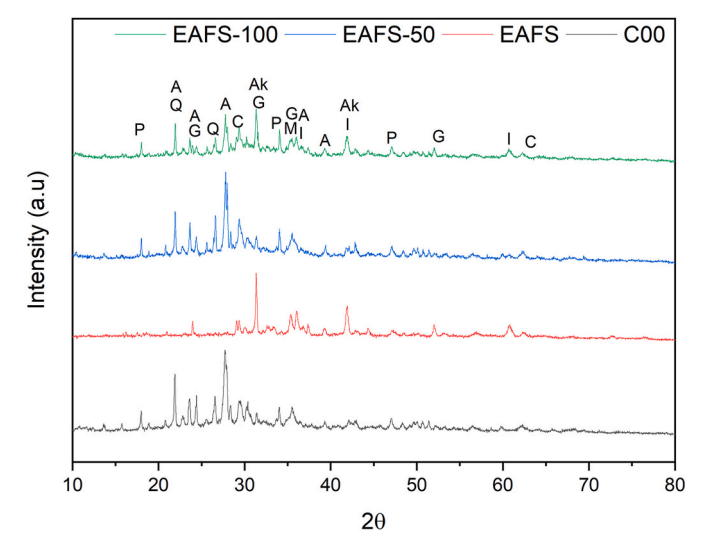


Fig. 16. X-ray diffraction (XRD) of concrete samples at 28 days. A: albite, Ak: å kermanite, C: calcite, G: gehlenite, I: wüstite, M: mellite, P: portlandite, Q: quartz.

13311-92, in relation to what is specified by Andreu and Miren (2014).

The respective increases of 4.95% and 14.37% for EAFS-50 and EAFS-100, compared to the control series, are associated with the high density that the EAFS aggregate delivers to the concrete; this is considerably greater than the NA, even when the proportion of steel slag aggregate is 50% (Maslehuddin et al., 2003). For González-Ortega et al. (2019), an increase in the UPV values may be the result of a good connection between the cement matrix and the aggregate in the ITZ, which is consistent with what can be observed in the SEM images in the microstructural evolution, where there is a concrete of low porosity and

good homogeneity. In this sense, Papachristoforou et al. (2020) mentioned that UPV values largely depend on the content and changes of voids in the sample, which is consistent with what was obtained in Figs. 8 and 10, where the porosity of the concrete decreases and the density increases compared to the control series, as the replacement percentage increases.

4.10. SEM analysis

Figs. 14 and 15 show the SEM images taken of the series EAFS-50 and EAFS-100 after 28 days of hardening, respectively. Although some pores are visible in the series with EAFS, a dense and homogeneous surface can still be observed in Figs. 14a and 15a. Additionally, from Fig. 15b, the angularity and rough texture of the EAFS particle can be noted. These properties, as well as the stiffness of the aggregate, are capable of increasing the bond strength and improving the interlock between the artificial aggregate and the cement matrix (Brand and Roesler, 2018).

4.11. XRD analysis

Fig. 16 shows the diffractometry for the different series studied (CO0, EAFS-50 and EAFS-100). The peaks evidenced in the three concrete series are quartz (Q), portlandite (P), and albite (A), which is related to the origin of the NA and hydration products of the cement used in the mixtures (Arivumangai et al., 2021; Majhi and Nayak, 2019; Saravanakumar et al., 2016; Kupwade-Patil et al., 2018). In the case of albite (a mineral in the plagioclase feldspar family associated with siliceous aggregate)s, it should be noted that this peak falls as EAFS is incorporated in concrete and is absent in the EAFS aggregate (Hsiao et al., 2017; Deng et al., 2010). On the other hand, peaks associated with this material appear, such as å kermanite (Ak), gehlenite (G) and wüstite (I), associated with minerals of the å kermanite-gehlenite series (Rashad, 2022; Adegoloye et al., 2016; Gómez-Casero et al., 2022). It should be

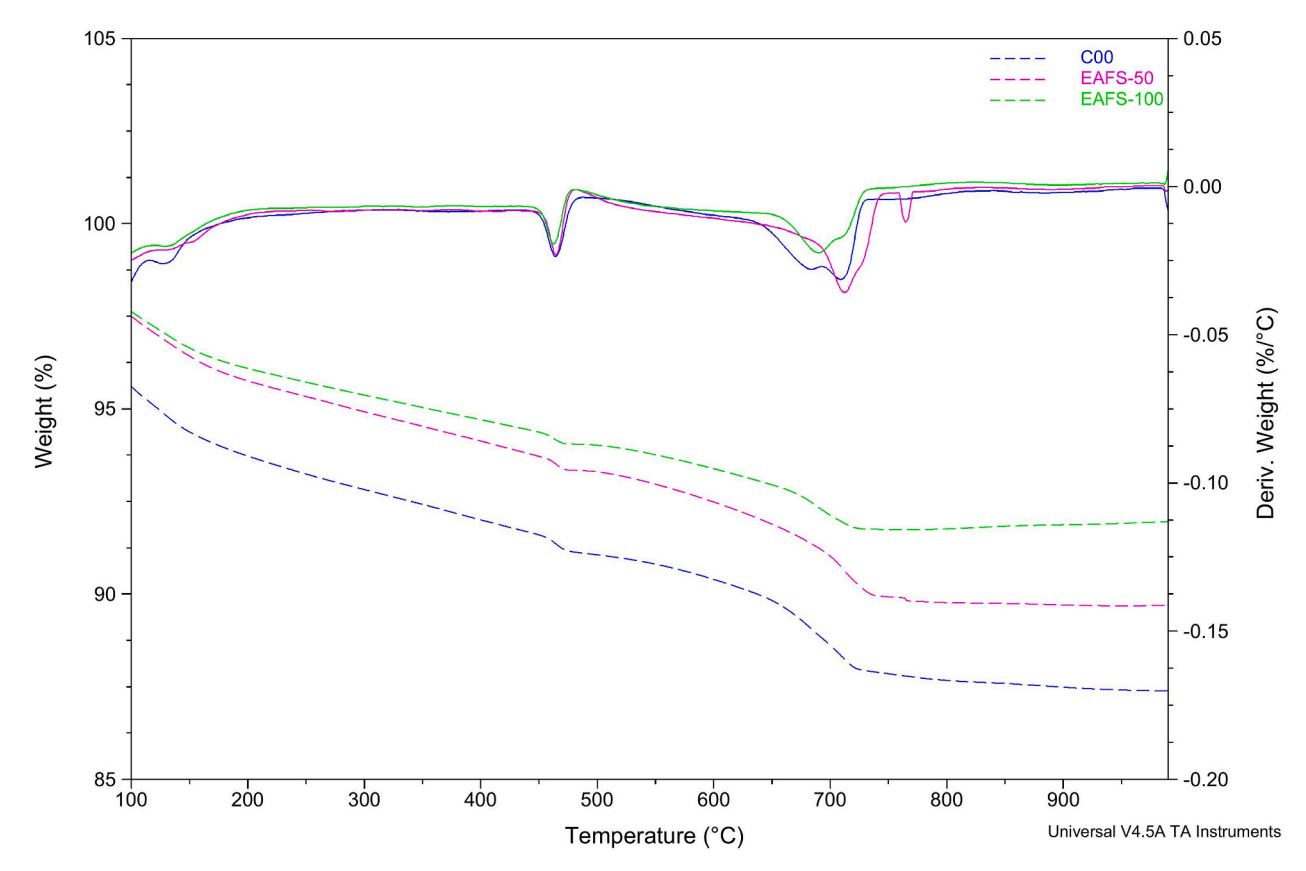


Fig. 17. TGA curves of concrete samples at 28 days.

Sample: EAFS2 Size: 67.3010 mg Method: Estandar

DSC-TGA

File: D:...\UFRO\ENSAYOS\TGA\EAFS2.001

Operator: FG

Run Date: 18-Jan-2023 11:40 Instrument: SDT Q600 V20.9 Build 20

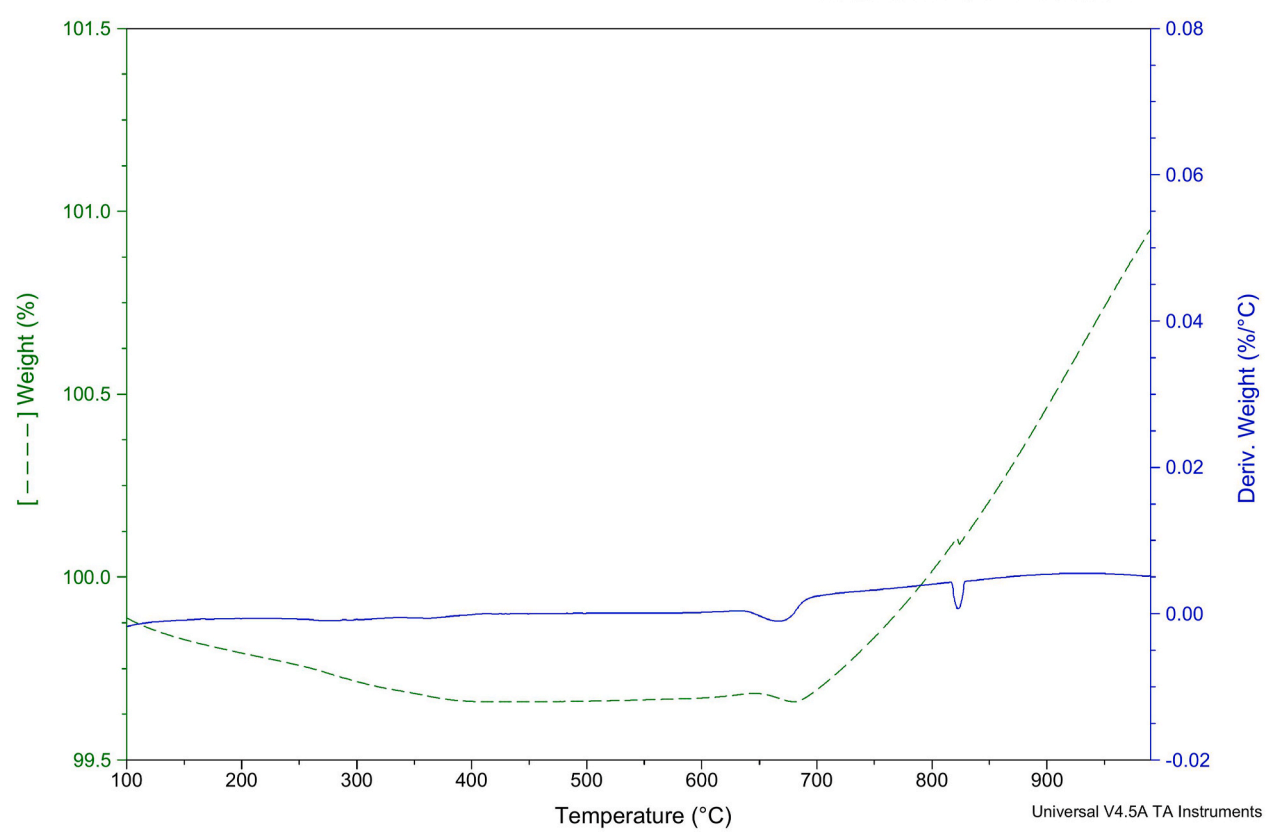


Fig. 18. TGA curves of EAFS aggregate.

emphasized that, because the EAFS used to manufacture the series passed through an 'aging process', no peaks of free CaO and MgO are observed in this case (Rashad, 2019). For this, it is also possible to distinguish peaks of calcite (C) in the diffraction pattern of the slag as well as in the samples of concrete that contain EAFS, since, being exposed to the atmosphere for months, there might be carbonation of the material because the calcite is among the main carbonate products formed by steel slag (Mo et al., 2016).

4.12. Thermogravimetric analysis (TGA)

A derived thermogravimetric analysis (DTG) was proposed to determine the behavior of the concrete at different temperatures and, in particular, to know the amount of Ca(OH)₂ present in the sample. Fig. 17 shows the TGA analysis of the samples studied (C00, EAFS-50 and EAFS-100), while Fig. 18 shows the TGA analysis of the EAFS aggregate used in the concrete mixes. The dissociation of the phases that contain H₂O is observed in three peaks with temperatures of 148 °C, 400 °C and 463 °C. Pan et al. (2016) encountered a similar behavior, which they attributed to evaporation of the surface water, evaporation of the interstitial water and dehydration of the crystalline water, respectively. The dehydration of calcium silicate hydrate (C-S-H) occurred at 200 °C and 400 °C for all the series. The peaks observed at 463 $^{\circ}\text{C}$ and 700 $^{\circ}\text{C}$ are attributed to the decomposition of the portlandite (Ca(OH)2) which occurs between 400 °C and 500 °C and the second peak above 550 °C is associated with calcite decomposition (CaCO₃), respectively, according to Morandeau et al. (2014). In the case of portlandite, the mass loss was very similar for all series because, in this case, its decomposition is not related to the type of aggregate used. This is not the case for calcite where, as shown in Fig. 16, the EAFS aggregate had a calcite peak which, added to its heterogeneity due to the fact that it comes from scrap used for the manufacture of recycled steel, resulted in a separate peak in the EAFS 50 series, which is also observed in its TGA test (see Fig. 18).

To accurately study the different phases present in EAFS is complex due to the difficulty in assigning a concrete crystalline structure in each phase, because these phases can form solid solutions and can present atom substitution at the same time. The different phases (compounds) can be in crystalline or amorphous form, with the latter being very common in EAFS. In the same way, the presence of different elements (Mn, Mg, Al, Ca, Si, Fe) in varying amounts in the slag makes the system remarkably difficult for their possible identification. The previous points relate to the chemical composition but it must be considered that the mineralogical composition depends on the aging or cooling processes applied to the by-product (Otegi Aldai, 2019).

5. Conclusions

In the search for construction materials focused on a circular economy, EAFS was incorporated as a coarse replacement aggregate to study its behavior in concretes. The following conclusions can be drawn from this research work.

• Water absorption and LA abrasion loss of the NA and the EAFS is within the Chilean standard (2% and 35% respectively); despite being slightly higher for EAFS, it does not present an appreciable loss in its properties. However, the densities increased up to 24.36%, which is why its weight must be considered for the preparation and use of concretes with EAFS.

- The workability decreased with the increase in EAFS replacement for NA; therefore, this must be considered when analyzing the type of concrete in which the EAFS will be used. Despite this, their use in conventional concretes is a viable option without having a negative impact on their resistive properties.
- A replacement of up to 100% of EAFS for NA resulted in a more rigid concrete, with greater compressive and flexural strength. At 28 days of curing, for the series EAFS-50 and EAFS-100, the compressive strength increased 8.97% and 30.90%, the flexural strength 17.99% and 35.71%, and the modulus of elasticity 5.05% and 25.02%, respectively.
- The presence of EAFS in concretes offers better behavior in their physical and mechanical properties because of its angularity and the rougher texture of the artificial aggregate, which gave a stronger adhesion to the cement matrix and improved their ITZ.
- The density, water absorption, porosity and UPV benefited from the EAFS replacement. In comparison to the control series, a full replacement of NA with EAFS increased density by 11.64% and UPV by 14.37%, while the water absorption and porosity decreased by 17.86% and 8.28%, respectively. In addition, the ultrasonic pulse velocity was greater than 4500 m/s for all the series tested, which is why they are classified as excellent.
- With respect to the chemical analysis, it should be mentioned that the DTG test presents similar curves for the peaks which are characteristic of decomposition of the cement. Meanwhile, the diffractometry of the XRD presents variations associated with the chemical composition of the EAFS.
- Given the generally good results obtained for EAFS as a coarse aggregate replacement, the present study may be considered as a starting point for carrying out further research in a national environment for the use of EAFS as fine aggregate and also its behavior and performance in structural elements to assess the capabilities and potential of the artificial aggregate.

Declaration of competing interest

The authors declare that they have no known competing financial interests or personal relationships that could have appeared to influence the work reported in this paper.

Acknowledgement

This work was supported by the Agencia Nacional de Investigación y Desarrollo de Chile (ANID) under Grant No. FONDECYT REGULAR 1211135.

References

- Abendeh, R.M., Salman, D., Al Louzi, R., 2022. Experimental and numerical investigations of interfacial bond in self-compacting concrete-filled steel tubes made with waste steel slag aggregates. Developments in the Built Environment 11, 100080. https://doi.org/10.1016/j.dibe.2022.100080. URL:
- Abu-Eishah, S.I., El-Dieb, A.S., Bedir, M.S., 2012. Performance of concrete mixtures made with electric arc furnace (EAF) steel slag aggregate produced in the Arabian Gulf region. Construct. Build. Mater. 34, 249–256.
- Adegoloye, G., Beaucour, A.L., Ortola, S., Noumowé, A., 2015. Concretes made of eaf slag and aod slag aggregates from stainless steel process: mechanical properties and durability. Construct. Build. Mater. 76, 313–321. https://doi.org/10.1016/J. CONBUILDMAT.2014.12.007.
- Adegoloye, G., Beaucour, A.-L., Ortola, S., Noumowe, A., 2016. Mineralogical composition of eaf slag and stabilised and slag aggregates and dimensional stability of slag aggregate concretes. Construct. Build. Mater. 115, 171–178. https://doi.org/ 10.1016/j.conbuildmat.2016.04.036.
- Ahmad, S., Iqbal, Y., Muhammad, R., 2017. Effects of coal and wheat husk additives on the physical, thermal and mechanical properties of clay bricks. Bol. Soc. Espanola Ceram, Vidr. 56. 131–138. https://doi.org/10.1016/j.bsecv.2017.02.001.
- Andrade, H.D., de Carvalho, J.M.F., Costa, L.C.B., Elói, F.P.d.F., e Silva, K.D.d.C., Peixoto, R.A.F., 2021. Mechanical performance and resistance to carbonation of steel slag reinforced concrete. Construct. Build. Mater. 298, 123910 https://doi.org/ 10.1016/j.conbuildmat.2021.123910.

- Andreu, G., Miren, E., 2014. Experimental analysis of properties of high performance recycled aggregate concrete. Construct. Build. Mater. 52, 227–235. https://doi.org/ 10.1016/j.conbuildmat.2013.11.054. URL:
- Anike, E.E., Saidani, M., Olubanwo, A.O., Anya, U.C., 2022. Flexural performance of reinforced concrete beams with recycled aggregates and steel fibres. Structures 39, 1264–1278. https://doi.org/10.1016/J.ISTRUC.2022.03.089. URL: https://linkingh.ub.elsevier.com/retrieve/pii/S2352012422002582.
- Arivumangai, A., Narayanan, R., Felixkala, T., 2021. Study on sulfate resistance behaviour of granite sand as fine aggregate in concrete through material testing and XRD analysis. Mater. Today Proc. 43, 1724–1729. https://doi.org/10.1016/j.matpr.2020.10.354. URL:
- Arribas, I., Santamaría, A., Ruiz, E., Ortega-López, V., Manso, J.M., 2015. Electric arc furnace slag and its use in hydraulic concrete. Construct. Build. Mater. 90, 68–79. https://doi.org/10.1016/J.CONBUILDMAT.2015.05.003.
- Ashish, D.K., Verma, S.K., 2019. Cementing efficiency of flash and rotary-calcined metakaolin in concrete. J. Mater. Civ. Eng. 31, 1–12. https://doi.org/10.1061/ (ASCE)MT.1943-5533.0002953. URL:
- Ashish, D.K., Verma, S.K., 2021. Robustness of self-compacting concrete containing waste foundry sand and metakaolin: a sustainable approach. J. Hazard Mater. 401, 123329 https://doi.org/10.1016/j.jhazmat.2020.123329. URL:
- ASTM C127-15, 2015. Standard Test Method for Relative Density (Specific Gravity) and Absorption of Coarse Aggregate. ASTM International, West Conshohocken, PA.
- ASTM C128-15, 2015. Standard Test Method for Relative Density (Specific Gravity), and Absorption of Fine Aggregate. ASTM International, West Conshohocken, PA.
- ASTM C131/C131M-20, 2020. Standard Test Method for Resistance to Degradation of Small-Size Coarse Aggregate by Abrasion and Impact in the Los Angeles Machine. ASTM International, West Conshohocken, PA.
- ASTM C136/C136M-19, 2019. Standard Test Method for Sieve Analysis of Fine and Coarse Aggregates. ASTM International, West Conshohocken, PA.
- ASTM C143/C143M-20, 2020. Standard Test Method for Slump of Hydraulic-Cement Concrete. ASTM International, West Conshohocken, PA.
- ASTM C1585-20, 2020. Standard Test Method for Measurement of Rate of Absorption of Water by Hydraulic Cement Concretes. ASTM International, West Conshohocken, PA.
- ASTM C31/C31M-19, 2019. Standard Practice for Making and Curing Concrete Test Specimens in the Field. ASTM International, West Conshohocken, PA.
- ASTM C39/C39M-21, 2021. Standard Test Method for Compressive Strength of Cylindrical Concrete Specimens. ASTM International, West Conshohocken, PA.
- ASTM C469/C469M-14, 2014. Standard Test Method for Static Modulus of Elasticity and Poisson's Ratio Concrete in Compression. ASTM International, West Conshohocken, PA
- ASTM C595/C595M-16, 2021. Standard Specification for Blended Hydraulic Cements.
 ASTM International, West Conshohocken, PA.
- ASTM C597-16, 2016. Standard Test Method for Pulse Velocity through Concrete. ASTM International, West Conshohocken, PA.
- ASTM C642-21, 2021. Standard Test Method for Density, Absorption, and Voids in Hardened Concrete. ASTM International, West Conshohocken, PA.
- ASTM C78/C78M-18, 2018. Standard Test Method for Flexural Strength of Concrete (Using Simple Beam with Third-Point Loading). ASTM International, West Conshohocken, PA.
- Biskri, Y., Achoura, D., Chelghoum, N., Mouret, M., 2017. Mechanical and durability characteristics of high performance concrete containing steel slag and crystalized slag as aggregates. Construct. Build. Mater. 150, 167–178. https://doi.org/10.1016/ j.conbuildmat.2017.05.083.
- Brand, A.S., Roesler, J.R., 2015. Steel furnace slag aggregate expansion and hardened concrete properties. Cement Concr. Compos. 60, 1–9. https://doi.org/10.1016/J. CEMCONCOMP.2015.04.006.
- Brand, A.S., Roesler, J.R., 2018. Interfacial transition zone of cement composites with steel furnace slag aggregates. Cement Concr. Compos. 86, 117–129. https://doi.org/ 10.1016/J.CEMCONCOMP.2017.11.012.
- Coppola, L., Buoso, A., Coffetti, D., Kara, P., Lorenzi, S., 2016. Electric arc furnace granulated slag for sustainable concrete. Construct. Build. Mater. 123, 115–119. https://doi.org/10.1016/J.CONBUILDMAT.2016.06.142.
- Deng, L., Liu, X., Liu, H., Dong, J., 2010. High-pressure phase relations in the composition of albite NaAlSi3O8 constrained by an ab initio and quasi-harmonic Debye model, and their implications. Earth Planet Sci. Lett. 298, 427–433. https://doi.org/10.1016/j.epsl.2010.08.008. URL:
- De Domenico, D., Faleschini, F., Pellegrino, C., Ricciardi, G., 2018. Structural behavior of RC beams containing EAF slag as recycled aggregate: numerical versus experimental results. Construct. Build. Mater. 171, 321–337. https://doi.org/10.1016/j. conbuildmat.2018.03.128.
- Faleschini, F., Alejandro Fernández-Ruíz, M., Zanini, M.A., Brunelli, K., Pellegrino, C., Hernández-Montes, E., 2015. High performance concrete with electric arc furnace slag as aggregate: mechanical and durability properties. Construct. Build. Mater. 101, 113–121. https://doi.org/10.1016/J.CONBUILDMAT.2015.10.022.
- Geiseler, J., 1996. Use of steelworks slag in Europe. Waste Manag. 16, 59–63. https://doi.org/10.1016/S0956-053X(96)00070-0.
- Gómez-Casero, M., Pérez-Villarejo, L., Sánchez-Soto, P., Eliche-Quesada, D., 2022. Comparative study of alkali activated cements based on metallurgical slags, in terms of technological properties developed. Sustainable Chemistry and Pharmacy 29, 100746. https://doi.org/10.1016/j.scp.2022.100746. URL:
- González-Ortega, M., Cavalaro, S., de Sensale, G.R., Aguado, A., 2019. Durability of concrete with electric arc furnace slag aggregate. Construct. Build. Mater. 217, 543–556. https://doi.org/10.1016/j.conbuildmat.2019.05.082.

- Hsiao, Y.H., La Plante, E.C., Krishnan, N.M., Le Pape, Y., Neithalath, N., Bauchy, M., Sant, G., 2017. Effects of irradiation on albite's chemical durability. J. Phys. Chem. A 121, 7835–7845. https://doi.org/10.1021/acs.jpca.7b05098.
- IS 2386-1, Methods of Test for Aggregates for Concrete, Part 1: Particle Size and Shape, 1963. Bureau of Indian Standards, Manak Bhawan, New Delhi.
- ISO 22007-2:2008(E), 2008. Plastics Determination of Thermal Conductivity and Thermal Diffusivity - Part 2: Transient Plane Heat Source (Hot Disc) Method. ISO, Geneva. CH.
- Jagadisha, A., Rao, K.B., Nayak, G., Kamath, M., 2021. Influence of nano-silica on the microstructural and mechanical properties of high-performance concrete of containing EAF aggregate and processed quarry dust. Construct. Build. Mater. 304, 124392 https://doi.org/10.1016/j.conbuildmat.2021.124392. URL:
- Khalaf, M.A., Ban, C.C., Ramli, M., Ahmed, N.M., Sern, L.J., Khaleel, H.A., 2020. Physicomechanical and gamma-ray shielding properties of high-strength heavyweight concrete containing steel furnace slag aggregate. J. Build. Eng. 30, 101306 https://doi.org/10.1016/j.jobe.2020.101306. URL:
- Kupwade-Patil, K., Palkovic, S.D., Bumajdad, A., Soriano, C., Büyüköztürk, O., 2018. Use of silica fume and natural volcanic ash as a replacement to Portland cement: micro and pore structural investigation using NMR, XRD, FTIR and X-ray microtomography. Construct. Build. Mater. 158, 574–590. https://doi.org/10.1016/j.conbuildmat.2017.09.165. URL:
- Letelier, V., Bustamante, M., Muñoz, P., Rivas, S., Ortega, J.M., 2021. Evaluation of mortars with combined use of fine recycled aggregates and waste crumb rubber. J. Build. Eng. 43, 103226 https://doi.org/10.1016/j.jobe.2021.103226.
- Lim, J.S., Cheah, C.B., Ramli, M.B., 2019. The setting behavior, mechanical properties and drying shrinkage of ternary blended concrete containing granite quarry dust and processed steel slag aggregate. Construct. Build. Mater. 215, 447–461. https://doi. org/10.1016/j.conbuildmat.2019.04.162. URL:
- Majhi, R., Nayak, A., 2019. Bond, durability and microstructural characteristics of ground granulated blast furnace slag based recycled aggregate concrete. Construct. Build. Mater. 212, 578-595. https://doi.org/10.1016/j.conbuildmat.2019.04.017.
- Manso, J.M., Polanco, J.A., Losañez, M., González, J.J., 2006. Durability of concrete made with eaf slag as aggregate. Cement Concr. Compos. 28, 528–534. https://doi. org/10.1016/J.CEMCONCOMP.2006.02.008.
- Marie, I., 2017. Thermal conductivity of hybrid recycled aggregate rubberized concrete. Construct. Build. Mater. 133, 516–524. https://doi.org/10.1016/j. conbuildmat.2016.12.113.
- Martins, A.C.P., Franco de Carvalho, J.M., Costa, L.C.B., Andrade, H.D., de Melo, T.V., Ribeiro, J.C.L., Pedroti, L.G., Peixoto, R.A.F., 2021. Steel Slags in Cement-Based Composites: an Ultimate Review on Characterization, Applications and Performance. https://doi.org/10.1016/j.conbuildmat.2021.123265.
- Maslehuddin, M., Sharif, A.M., Shameem, M., Ibrahim, M., Barry, M.S., 2003. Comparison of properties of steel slag and crushed limestone aggregate concretes. Construct. Build. Mater. 17, 105–112. https://doi.org/10.1016/S0950-0618(02) 00095-8
- Mo, L., Zhang, F., Deng, M., 2016. Mechanical performance and microstructure of the calcium carbonate binders produced by carbonating steel slag paste under CO2 curing. Cement Concr. Res. 88, 217–226. https://doi.org/10.1016/j. cemconres.2016.05.013. URL:
- Monosi, S., Ruello, M.L., Sani, D., 2016. Electric arc furnace slag as natural aggregate replacement in concrete production. Cement Concr. Compos. 66, 66–72. https://doi. org/10.1016/J.CEMCONCOMP.2015.10.004.
- Morandeau, A., Thiéry, M., Dangla, P., 2014. Investigation of the carbonation mechanism of ch and c-s-h in terms of kinetics, microstructure changes and moisture properties. Cement Concr. Res. 56, 153–170. https://doi.org/10.1016/j. cemconres.2013.11.015.
- Motz, H., Geiseler, J., 2001. Products of steel slags an opportunity to save natural resources. Waste Manag. 21, 285–293. https://doi.org/10.1016/S0956-053X(00) 00102-1.
- Oikonomou, N.D., 2005. Recycled concrete aggregates. Cement Concr. Compos. 27, 315-318.
- Ortega-López, V., Fuente-Alonso, J.A., Santamaría, A., San-José, J.T., Aragón, Á., 2018. Durability studies on fiber-reinforced EAF slag concrete for pavements. Construct. Build. Mater. 163, 471–481. https://doi.org/10.1016/j.conbuildmat.2017.12.121.
- Otegi Aldai, K., 2019. Estudio de la escoria de acería de HAE: aspectos expansivos y ambientales. Ph.D. thesis. Universitat Politècnica de Catalunya.
- Özalp, F., 2022. Effects of electric arc furnace (eaf) slags on mechanical and permeability properties of paving stone, kerb and concrete pipes. Construct. Build. Mater. 329, 127159 https://doi.org/10.1016/j.conbuildmat.2022.127159.

- Pan, S.-Y., Chang, E.-E., Kim, H., Chen, Y.-H., Chiang, P.-C., 2016. Validating carbonation parameters of alkaline solid wastes via integrated thermal analyses: principles and applications. J. Hazard Mater. 307, 253–262. https://doi.org/10.1016/j. ibazmat.2015.12.065
- Papachristoforou, M., Anastasiou, E.K., Papayianni, I., 2020. Durability of steel fiber reinforced concrete with coarse steel slag aggregates including performance at elevated temperatures. Construct. Build. Mater. 262, 120569 https://doi.org/ 10.1016/J.CONBUILDMAT.2020.120569.
- Pellegrino, C., Gaddo, V., 2009. Mechanical and durability characteristics of concrete containing EAF slag as aggregate. Cement Concr. Compos. 31, 663–671. https://doi. org/10.1016/J.CEMCONCOMP.2009.05.006.
- Pellegrino, C., Cavagnis, P., Faleschini, F., Brunelli, K., 2013. Properties of concretes with black/oxidizing Electric Arc furnace slag aggregate. Cement Concr. Compos. 37, 232–240. https://doi.org/10.1016/J.CEMCONCOMP.2012.09.001.
- Qasrawi, H., Shalabi, F., Asi, I., 2009. Use of low CaO unprocessed steel slag in concrete as fine aggregate. Construct. Build. Mater. 23, 1118–1125. https://doi.org/10.1016/ i.conbuildmat.2008.06.003. URL:
- Rashad, A.M., 2019. A synopsis manual about recycling steel slag as a cementitious material. J. Mater. Res. Technol. 8, 4940–4955. https://doi.org/10.1016/j. imrt.2019.06.038. URL:
- Rashad, A.M., 2022. Behavior of steel slag aggregate in mortar and concrete a comprehensive overview. J. Build. Eng. 53, 104536 https://doi.org/10.1016/J. LOBE 2022 104536
- Ratajczak, E., Bidzińska, G., Szostak, A., Herbeć, M., 2015. Resources of post-consumer wood waste originating from the construction sector in Poland, Resources. Conserv. Recycl. 97, 93–99. https://doi.org/10.1016/J.RESCONREC.2015.02.008.
- Revilla-Cuesta, V., yan Shi, J., Skaf, M., Ortega-López, V., Manso, J.M., 2022. Non-destructive Density-Corrected Estimation of the Elastic Modulus of Slag-Cement Self-Compacting Concrete Containing Recycled Aggregate, Developments in the Built Environment 12, 100097. https://doi.org/10.1016/j.dibe.2022.100097. URL: https://linkinghub.elsevier.com/retrieve/pii/S266616592200031X.
- Santamaría, A., Orbe, A., San José, J.T., González, J.J., 2018. A study on the durability of structural concrete incorporating electric steelmaking slags. Construct. Build. Mater. 161, 94–111. https://doi.org/10.1016/J.CONBUILDMAT.2017.11.121.
- Santamaría, A., Ortega-López, V., Skaf, M., Chica, J.A., Manso, J.M., 2020. The study of properties and behavior of self compacting concrete containing Electric Arc Furnace Slag (EAFS) as aggregate. Ain Shams Eng. J. 11, 231–243. https://doi.org/10.1016/j.asej.2019.10.001.
- Santamaría, A., Romera, J.M., Marcos, I., Revilla-Cuesta, V., Ortega-López, V., 2021. Shear strength assessment of reinforced concrete components containing EAF steel slag aggregates. J. Build. Eng., 103730 https://doi.org/10.1016/J. JOBE.2021.103730. URL:
- Santamaría, A., Romera, J.M., Marcos, I., Revilla-Cuesta, V., Ortega-López, V., 2022. Shear strength assessment of reinforced concrete components containing EAF steel slag aggregates. J. Build. Eng. 46, 103730 https://doi.org/10.1016/J. JOBE 2021.103730.
- Saravanakumar, P., Abhiram, K., Manoj, B., 2016. Properties of treated recycled aggregates and its influence on concrete strength characteristics. Construct. Build. Mater. 111, 611–617. https://doi.org/10.1016/j.conbuildmat.2016.02.064. URL:
- Saxena, S., Tembhurkar, A., 2018. Impact of use of steel slag as coarse aggregate and wastewater on fresh and hardened properties of concrete. Construct. Build. Mater. 165, 126–137. https://doi.org/10.1016/j.conbuildmat.2018.01.030.
- Singh, P., Roy, A.D., Singh, H., 2022. Mechanical and durability properties of concrete incorporating weathered coarse Linz-Donawitz (LD) steel slag. J. Build. Eng. 61, 105301 https://doi.org/10.1016/j.jobe.2022.105301. URL:
- U.S. Geological Survey, 2022. Miner. Commod. Summ. 2022.
- Wang, Q., Yan, P., Yang, J., Zhang, B., 2013. Influence of steel slag on mechanical properties and durability of concrete. Construct. Build. Mater. 47, 1414–1420. https://doi.org/10.1016/J.CONBUILDMAT.2013.06.044.
- Xu, X., Wang, Y., Tao, L., 2019. Comprehensive evaluation of sustainable development of regional construction industry in China. J. Clean. Prod. 211, 1078–1087. https://doi. org/10.1016/J.JCLEPRO.2018.11.248.
- Zanini, M.A., 2019. Structural reliability of bridges realized with reinforced concretes containing electric arc furnace slag aggregates. Eng. Struct. 188, 305–319. https://doi.org/10.1016/J.ENGSTRUCT.2019.02.052.
- Zhang, X., Zhao, S., Liu, Z., Wang, F., 2019. Utilization of steel slag in ultra-high performance concrete with enhanced eco-friendliness. Construct. Build. Mater. 214, 28–36. https://doi.org/10.1016/J.CONBUILDMAT.2019.04.106.